ISSN 1070-4272, Russian Journal of Applied Chemistry, 2021, Vol. 94, No. 9, pp. 1302–1312. © Pleiades Publishing, Ltd., 2021.

CATALYSIS

Methanol Dehydrogenation to Methyl Formate Catalyzed by Cu/SiO_2 Catalysts: Impact of Precipitation Procedure and Calcination Temperature

A. L. Wang[a], C. L. Ye[a], X. Y. Jia[a], and H. B. Yin[a,*]

[a] *Faculty of Chemistry and Chemical Engineering, Jiangsu University, Zhenjiang, 212013 China*
**e-mail: yin@ujs.edu.cn*

Received May 17, 2021; revised November 1, 2021; accepted November 10, 2021

Abstract—Considered three options for the synthesis of a catalyst by the precipitation method, the Cu/SiO_2 catalysts prepared by varying the precipitation procedure and calcination temperature for the dehydrogenation of methanol was investigated. When the CuO/SiO_2 catalyst precursors were prepared by the addition of a copper nitrate aqueous solution into an ammonia aqueous solution (reverse precipitation) and co-current flow addition of both aqueous solutions, after reduction with gaseous hydrogen, small-sized metallic copper nanocrystallites were formed in the reduced Cu/SiO_2 catalysts as compared to those prepared by the addition of an ammonia aqueous solution into a copper nitrate aqueous solution (direct precipitation). The reduced Cu/SiO_2 catalysts prepared by the reverse precipitation method with relatively lower acidity and basicity exhibited higher catalytic activity for the formation of methyl formate in methanol dehydrogenation. The reduced Cu/SiO_2 catalysts prepared by the calcination at a lower temperature exhibited higher catalytic activity for the formation of methyl formate. The surface metallic Cu^0 and Cu^+ species catalyzed the methanol dehydrogenation to methyl formate, meanwhile the surface Cu^+ cations enhanced the decomposition of the resultant methyl formate to CO and H_2.

Keywords: Cu/SiO_2 catalyst, dehydrogenation, methyl formate, methanol

DOI: 10.1134/S1070427221090135

INTRODUCTION

Supported copper catalysts exhibited good catalytic activities in the hydrogenation, dehydrogenation, methanol synthesis, and water gas shift reactions [1–11]. Among the reactions mentioned-above, the direct dehydrogenation of methanol to methyl formate has become an attractive direction in C1 chemical industry and also attracted a great attention of researchers because this reaction process is more economical and environmentally friendly as compared with the other routes, such as esterification of methanol and formic acid [12], liquid phase methanol carbonylation [13], and oxidative dehydrogenation of methanol [14]. Gas phase dehydrogenation of methanol catalyzed by copper-based catalyst mainly consists of two successive reactions (Eqs. 1 and 2).

$$2CH_3OH \rightarrow HCOOCH_3 + 2H_2, \quad (1)$$

$$HCOOCH_3 \rightarrow 2CO + 2H_2. \quad (2)$$

The byproducts, CO and H_2 are formed with a CO/H_2 mole ratio of 1 : 2, which is the same as that in the stoichiometry of methanol synthesis by the reaction between CO and H_2. It was suggested that metallic Cu^0 species were the active sites in the catalytic methanol dehydrogenation to methyl formate [15–22]. The properties of the supports had significant effects on the catalytic activities of the supported metallic Cu catalysts, such as Cu/Sapo [16], Cu/Mont [16], Cu/hydroxyapatite [17], Cu/MgO [17], Cu/C [18], Cu/SiO_2 [17, 19, 21, 22], and Cu/chromite [20]. These supports with either acidity or basicity improved the methanol conversion, but decreased the methyl formate selectivity. It was suggested that the acidic sites favored the intermolecular dehydration of methanol to dimethyl ether and that the basic sites could cause the rapid decomposition of resultant methyl formate to CO and H_2 [17]. The neutral

silica-supported metallic copper catalysts favored the formation of methyl formate.

Although the chemical states of copper species and surface properties of the supports have significant effects on the direct dehydrogenation reaction of methanol, the effects of preparation procedure and calcination temperature on the properties of the supported copper catalysts as well as their catalytic activity is still worthy of investigation in detail [23–25].

In our present work, a series of Cu/SiO_2 catalysts were prepared by different precipitation procedures and calcined at different temperatures by using copper nitrate as the copper source, SiO_2 aerogel as the support, and ammonia as the precipitant. The chemical structures and acid/base performance of the reduced Cu/SiO_2 catalysts were investigated by XRD, XPS, N_2 adsorption/desorption, CO_2-TPD, and NH_3-TPD techniques. The relationship between the catalyst structures and the catalytic activity in the methanol dehydrogenation reaction was discussed.

EXPERIMENTAL

Chemicals

Copper nitrate trihydrate ($Cu(NO_3)_2 \cdot 3H_2O$), ammonia solution (28 wt %), methanol, methyl formate were purchased from Sinopharm Chemical Reagent Co., Ltd. Silica aerogel (SiO_2, 160 $m^2\ g^{-1}$) was purchased from Jiangsu Haoneng Chemical Co., Ltd. All the chemicals were of reagent grade.

Catalyst Preparation

A series of Cu/SiO_2 catalysts were prepared by different precipitation procedures at room temperature and then calcined at various temperatures. The preparation procedures are illustrated in Scheme 1.

Process I: an ammonia (0.5 M, 122 mL) aqueous solution was added dropwise into a copper nitrate (0.1 M, 315 mL) aqueous solution until the pH value of the reaction mixture was increased to 6.5. After aging at 60°C for 2 h, 18 g of SiO_2 aerogel was added into the above-mentioned suspension and stirred for 2 h. The as-prepared catalyst precursors were filtrated, washed with deionized water, dried at 120°C for 12 h, and then calcinated at 350, 450, 550, and 650°C for 4 h, respectively. The calcined catalyst was denoted as CuO/SiO_2-I. After reduction with gaseous hydrogen, the reduced catalysts were denoted as Cu/SiO_2-I. The

Scheme 1. The preparation procedures of the Cu/SiO_2 catalysts.

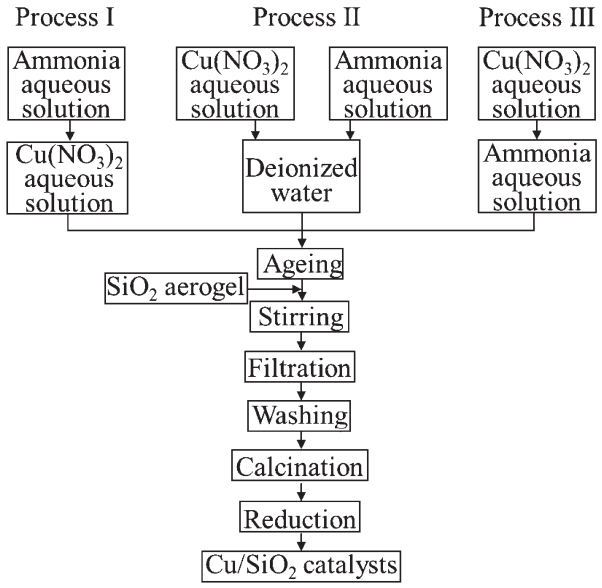

weight percentage of metallic copper in the catalysts was 10 wt %. The catalyst preparation method is called as the direct precipitation method in the context.

Process II: ammonia (0.5 M, 122 mL) and copper nitrate (0.1 M, 315 mL) aqueous solutions were simultaneously added dropwise into 200 mL of deionized water. The pH value of reaction mixture was kept at 6.5 by changing the flow rate of ammonia solution. The subsequent procedures were the same as those mentioned in the process I. The as-prepared catalysts were denoted as Cu/SiO_2-II with a metallic copper percentage of 10 wt %. The catalyst preparation method is called the co-current flow precipitation method in the context.

Process III, a copper nitrate (0.1 M, 315 mL) aqueous solution was added dropwise into an ammonia aqueous solution (0.5 M, 150 mL). After adding copper nitrate aqueous solution, the pH value of the suspension was adjusted to 6.5 by adding a nitric acid aqueous solution (0.5 M). The as-prepared catalysts were denoted as Cu/SiO_2-III with a metallic copper percentage of 10 wt %. The catalyst preparation method is called as the reverse precipitation method in the context.

Characterization of Catalyst

Powder X-ray diffraction was applied to measure the bulk chemical structures of the precipitates, calcined CuO/SiO_2 precursors, and reduced Cu/SiO_2 catalysts. The XRD data of the samples were recorded on an

Scheme 2. The flow chart of catalysis apparatus.

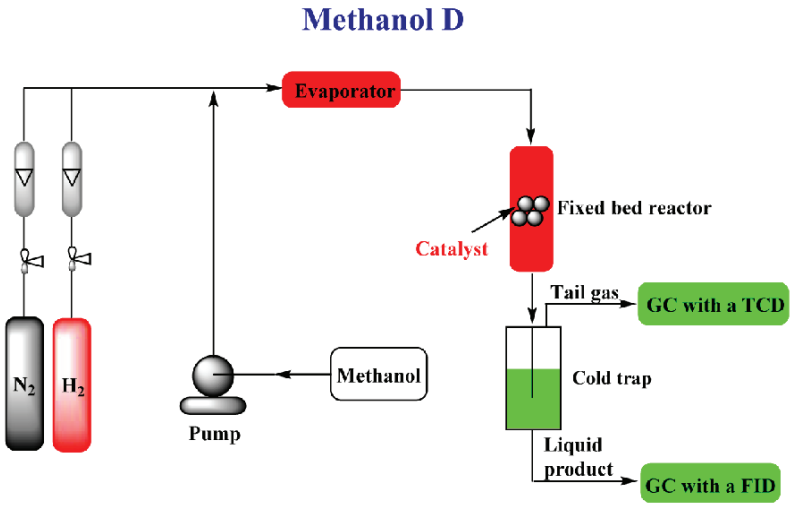

X-ray diffractometer (D8 super speed Bruker-Apex) using CuK_α radiation (λ = 1.54056 Å) with Ni filter. The crystallite sizes of CuO and Cu were calculated by the Scherrer's equation. The calculation was carried out by the peak (111).

The X-ray photoelectron spectra of the controlled metallic Cu sample prepared according to the process III, SiO_2 aerogel, calcined CuO/SiO_2, and reduced Cu/SiO_2 catalysts were recorded on an ESCALAB 250Xi spectrometer. The binding energies of the elements were corrected with respect to the C1*s* peak at 284.6 eV.

The surface acidity and basicity of the reduced Cu/SiO_2 catalyst were measured in a micro-reactor under atmospheric pressure by using the NH_3- and CO_2-TPD techniques. For the acidity measurement, the reduced Cu/SiO_2 catalyst (0.1 g) was firstly dried at 120°C for 40 min in a N_2 stream, and then saturated with pure NH_3 for 30 min. After purging with helium (30 mL min^{-1}) at 100°C for 40 min to remove the physically adsorbed NH_3, the sample was heated at a linear heating rate of 10°C min^{-1} up to 750°C. For the basicity measurement, the reduced Cu/SiO_2 catalyst (0.1 g) was saturated with pure CO_2 for 40 min after drying at 120°C for 40 min in a N_2 stream. After purging with helium (30 mL min^{-1}) at 100°C for 40 min to remove the physically adsorbed CO_2, the sample was heated at a linear heating rate of 10°C min^{-1} up to 750°C. The desorption amounts of NH_3 and the CO_2 were quantitatively calibrated by pure NH_3 and CO_2 samples, respectively.

The specific surface areas of reduced Cu/SiO_2 catalysts were measured by the N_2 adsorption/desorption method at –196°C using a Quantachrome Nova 2000E Surface Area, Pore Size Analyzer and BET calculation method. The samples were degassed at 120°C in a N_2 flow for 3 h to remove the physically adsorbed water in situ before the measurement.

Catalytic Test

Dehydrogenation reaction of methanol to methyl formate was carried out in a stainless steel fixed-bed reactor with an inside diameter of 8 mm and a length of 200 mm. The apparatus is shown in Scheme 2. Calcined CuO/SiO_2 precursor (3 g) with the particle sizes ranging from 20–40 mesh was packed in the reactor. The reaction was conducted at the temperatures ranging from 200 to 280°C under the atmospheric pressure. Before catalytic test, the CuO/SiO_2 precursor was reduced in a mixed H_2/N_2 (1 : 9, v/v) stream (100 mL min^{-1}) from the room temperature (25°C) to 280°C at a heating rate of 10°C min^{-1}. When the reduction temperature reached 280°C, the catalyst was continuously reduced at this temperature for 4 h in a mixed H_2/N_2 (3 : 7, v/v) stream at a flow rate of 100 mL min^{-1}.

For the catalytic test, a stream of liquid methanol was firstly fed into an evaporator at 200°C with a flow rate of 6 mL h^{-1}, and then the vaporized methanol was fed into the reactor. The liquid phase products were condensed and collected in a cooling trap at –20°C. The flow rate of gas phase products was measured with a float meter. The reaction products were analyzed on two gas chromatographs, one with an FID and a PEG-

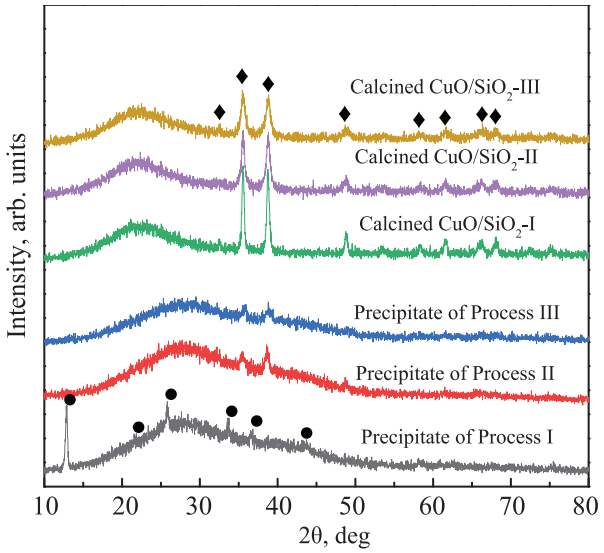

Fig. 1. XRD patterns of the precipitates prepared by different precipitation procedures and the CuO/SiO_2 precursors calcined at 350°C for 4 h. (●) $Cu_2(OH)_3NO_3$; (♦) CuO.

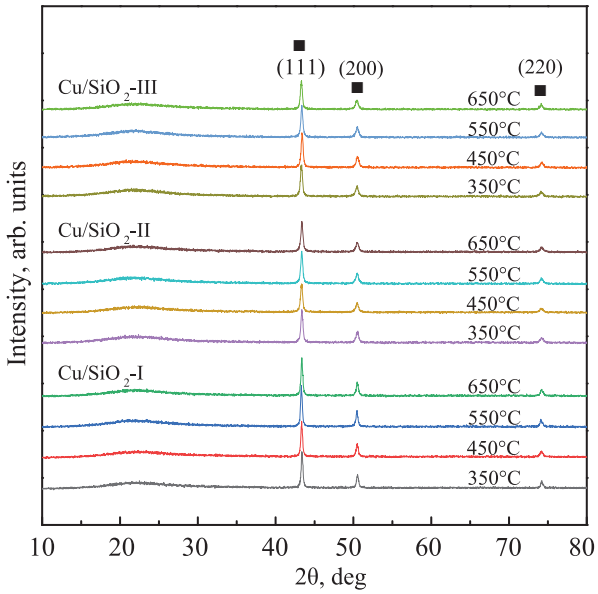

Fig. 2. XRD patterns of the reduced Cu/SiO_2 catalysts prepared by different precipitation procedures at different calcination temperatures. (■) Metallic Cu^0.

20M capillary column for the analysis of the liquid phase products and the other with a TCD and a TDX-01 packed column for the analysis of tail gas. The product selectivity was calculated according to carbon balance. The methanol conversion (%) and product selectivity (%) were calculated according to the following equations:

$$X_{\mathrm{MeOH}} = \left(n_{0,\mathrm{MeOH}} - n_{\mathrm{t,MeOH}}\right) / n_{0,\mathrm{MeOH}} \times 100, \quad (3)$$

$$S_{\mathrm{MF}} = 2n_{\mathrm{MF}} \left(n_{0,\mathrm{MeOH}} - n_{\mathrm{t,MeOH}}\right) \times 100, \quad (4)$$

$$S_{\mathrm{CO}} = n_{\mathrm{CO}} \left(n_{0,\mathrm{MeOH}} - n_{\mathrm{t,MeOH}}\right) \times 100, \quad (5)$$

where, X_{MeOH} is the methanol conversion, S_{MF} and S_{CO} are the selectivities of methyl formate and carbon monoxide, respectively. $n_{0,\mathrm{MeOH}}$ is the mole number of methanol fed for 1 h, $n_{\mathrm{t,MeOH}}$ is the mole number of methanol collected for 1 h in a cold trap, n_{CO} is the mole number of carbon monoxide produced for 1 h in tail gas. The catalysis experiments were repeated at least three times and the experimental errors were ±5%.

RESULTS AND DISCUSSION

Chemical Structures of Precipitate, Calcined Cu/SiO_2 Precursor, and Reduced Cu/SiO_2 Catalyst

The XRD patterns of the precipitates prepared by the direct (process I), co-current flow (process II), and reverse (process III) precipitation methods are shown in Fig. 1. When the precipitate was prepared by the process I, the XRD peaks appeared at (2θ) 12.8, 21.6, 25.8, 33.5, 36.5, and 43.5°, respectively. These peaks were ascribed to those of the $Cu_2(OH)_3NO_3$ (JCPDS 15-0014). For the precipitates prepared by the processes II and III, two weak peaks appearing at (2θ) 35.5° and 38.7° were observed, indicating that the precipitates had the CuO phase (JCPDS 48-1548).

After calcination at 350°C for 4 h, the XRD peaks of all the representative calcined CuO/SiO_2 precursors appeared at 32.5, 35.5, 38.7, 48.7, 58.2, 61.5, 66.2, and 68.1°, respectively, which were ascribed to those of the standard CuO (JCPDS 48-1548) (Fig. 1). The XRD peak intensity of CuO of the calcined CuO/SiO_2-I was stronger than those of the calcined CuO/SiO_2-II and CuO/SiO_2-III. The crystallite size (111) of CuO of the calcined CuO/SiO_2-I was 21 nm, which was obviously larger than those of the CuO/SiO_2-II and CuO/SiO_2-III (15 and 14 nm). The results indicated that the co-current flow and reverse precipitation processes favored the formation of small-sized CuO crystallites as compared to the direct precipitation process.

The XRD peaks of all the reduced Cu/SiO_2 catalysts appeared at (2θ) 43.3, 50.4, and 74.2°, respectively, which were consistent with those of the face centered cubic metallic copper (JCPDS 04-0836) (Fig. 2). No peaks of copper oxides or hydroxides were detected, indicating that the CuO species were completely reduced to metallic Cu^0 under our present reduction condition.

Scheme 3. Evolution mechanisms of metallic Cu^0 crystallites in Cu/SiO_2 catalysts.

(1) The co-current flow or reverse precipitation method:

$$Cu^{2+} + NH_3 \cdot H_2O \xrightarrow{\text{Precipitation}} Cu^{2+}\text{-}NH_3 \text{ complex} \xrightarrow{\text{Precipitation}} \text{CuO precipitate}$$

$$\xrightarrow{\text{Calcination}} \text{Small-sized CuO} \xrightarrow{\text{Reduction}} \text{Small sized metallic } Cu^0$$

(2) The co-current flow or reverse precipitation method:

$$Cu^{2+} + OH^- \xrightarrow{\text{Precipitation}} Cu_2(OH)_3NO_3 \text{ precipitate} \xrightarrow{\text{Calcination}} \text{Large-sized CuO}$$

$$\xrightarrow{\text{Reduction}} \text{Large-sized metallic } Cu^0$$

The crystallite sizes of Cu^0 (111) in the reduced Cu/SiO_2 catalysts were calculated by the Scherrer's equation (Table 1). When the CuO/SiO_2-I precursors were prepared by the calcination at 350–650°C, the crystallites sizes of the metallic Cu^0 (111) of the reduced Cu/SiO_2-I catalysts were in a range of 31.1–33.4 nm.

When the CuO/SiO_2-II and CuO/SiO_2-III precursors were prepared by the calcination at 350–650°C, the crystallites sizes of the metallic Cu^0 species (111) of the reduced Cu/SiO_2-II and Cu/SiO_2-III catalysts ranged from 26.3 to 27.0 and 26.0 to 27.0 nm, respectively.

It is interesting to find that the precipitation procedures obviously affected the crystallite sizes of metallic Cu^0 species of the reduced Cu/SiO_2 catalysts. The direct precipitation caused the formation of the metallic copper species with large crystallite sizes whereas the co-current flow and reverse precipitation procedures were beneficial to the formation of the metallic copper species with small crystallite sizes. It could be explained as that the co-current flow and reverse precipitation processes could supply a surrounding of abundant NH_3 molecules, resulting in the formation of Cu^{2+}-NH_3 complexes and subsequent formation of small-sized CuO precipitate. After calcination and reduction, the small-sized metallic Cu^0 nanocrystallites were formed (Scheme 3).

In the direct precipitation process, the lower basicity at a local precipitation zone was beneficial to the formation of $Cu_2(OH)_3NO_3$ precipitates, giving the formation of large-sized CuO crystallites in the calcination process. After reducing with H_2, the large-sized metallic Cu^0 nanocrystallites were formed (Scheme 3).

Surface Chemical State of Copper Species of Reduced Cu/SiO_2 Catalyst

The XPS measurement was utilized to analyze the surface chemical states of the controlled metallic Cu sample and representative reduced Cu/SiO_2 catalysts (Fig. 3). The CuO/SiO_2 precursors were prepared by

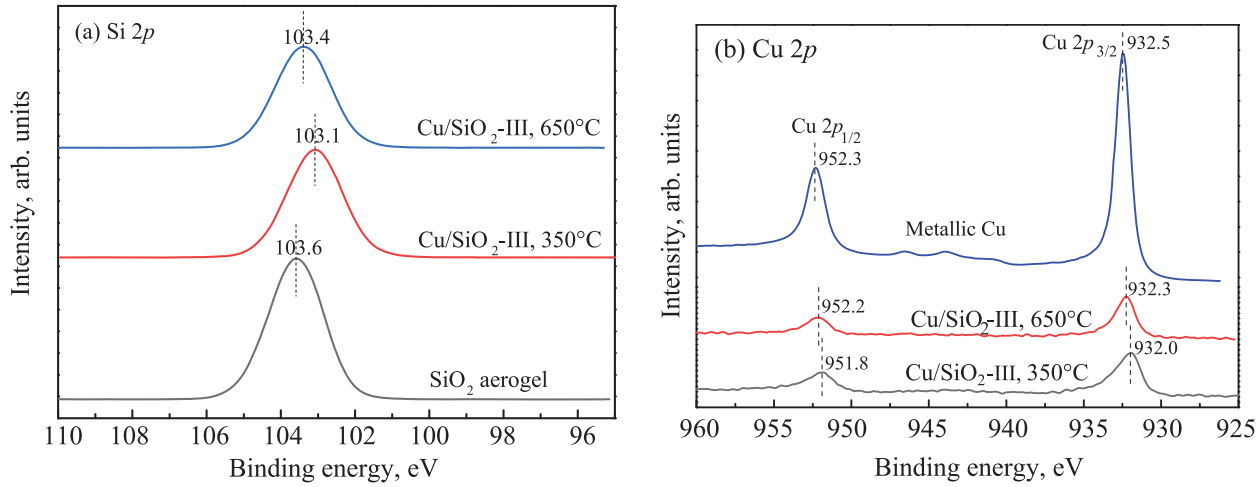

Fig. 3. XPS of (a) Si2*p* and (b) Cu2*p* of the SiO_2 aerogel, controlled metallic Cu, and reduced Cu/SiO_2-III catalysts. The CuO/SiO_2-III precursors were calcined at 350 and 650°C for 4 h, respectively.

the reverse precipitation method and calcinated at 350 and 650°C for 4 h, respectively. The reduced Cu/SiO_2 catalysts were denoted as Cu/SiO_2-III-350°C and Cu/SiO_2-III-650°C, respectively.

In comparation, the controlled metallic Cu sample was prepared according to the process III procedures. The controlled CuO precursor was calcined at 350°C for 4 h and reduced at 280°C in a H_2/N_2 (3 : 7, v/v) stream for 4 h.

The binding energies of Si2*p* of the SiO_2 aerogel, reduced Cu/SiO_2-III-350°C, and Cu/SiO_2-III-650°C catalysts were 103.6, 103.1, and 103.4 eV, respectively. The binding energies of Cu2*p*1/2 and Cu2*p*3/2 of the controlled metallic Cu sample, reduced Cu/SiO_2-III-350°C, and Cu/SiO_2-III-650°C catalysts were 952.3, 932.5; 951.8, 932; and 952.2, 932.3 eV, respectively. The binding energy shifts of Cu2*p* and Si2*p* were observed in the reduced Cu/SiO_2 catalysts as compared to those of the controlled metallic Cu and SiO_2 aerogel samples, respectively. It was suggested that there was an interaction between SiO_2 support and metallic Cu species.

No satellite peak of Cu^{2+} located at *ca*. 942 eV was observed in the XPS of these samples, revealing that the Cu^{2+} species were completely reduced to metallic Cu^0 and/or Cu^+ [26,27].

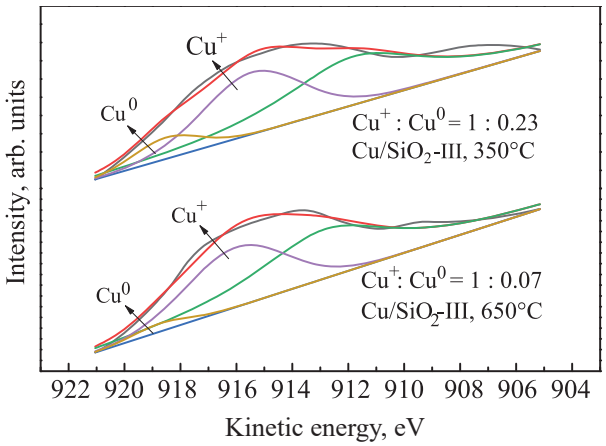

Fig. 4. XAES of Cu LMM of the reduced Cu/SiO_2 catalysts.

To analyze the surface oxidation state of the Cu species in the reduced Cu/SiO_2 catalysts, the surface composition of the Cu^+ and Cu^0 species was determined by the X-ray excited Auger electron spectroscopy (XAES). The Cu LMM XAES of the reduced Cu/SiO_2 catalysts are shown in Fig. 4. According to the literature, the XAES peaks of the Cu^+ and Cu^0 species centered at 916 and 918.7 eV, respectively [28–32]. A peak at *ca*. 912 eV was used to eliminate the effect of other orbital electrons on the XAES [25]. The XAES peaks of the reduced Cu/SiO_2 catalysts were deconvoluted into three

Table 1. Physicochemical properties of the reduced Cu/SiO_2 catalysts

Catalysts	Calcination temperatures, °C	Crystallite sizes of Cu^0 (111), nm	Specific areas, $m^2\ g^{-1}$	Pore diameters, nm	Total acidities, μmol NH_3/g_{cat}	Total basicities, μmol CO_2/g_{cat}
SiO_2 aerogel	350				59.5	10.7
	450				36.9	6.9
	550				21.9	4.7
	650				19.4	4.0
Cu/SiO_2-I	350	32.1	154.5	14.6	1512.7	462.0
	450	33.4	156.4	16.0	1438.4	405.2
	550	32.6	160.4	14.6	1236.8	259.6
	650	31.1	150.5	14.8	959.1	230.9
Cu/SiO_2-II	350	26.3	156.6	14.6	2113.7	719.8
	450	26.3	159.5	15.2	1794.8	643.6
	550	26.3	160.5	15.0	1693.8	567.8
	650	27.0	155.9	14.8	1537.7	313.6
Cu/SiO_2-III	350	26.0	147.0	16.7	781.7	506.6
	450	27.0	155.7	15.7	518.3	448.8
	550	26.8	151.0	16.5	475.2	378.6
	650	26.8	146.9	15.5	429.1	326.1

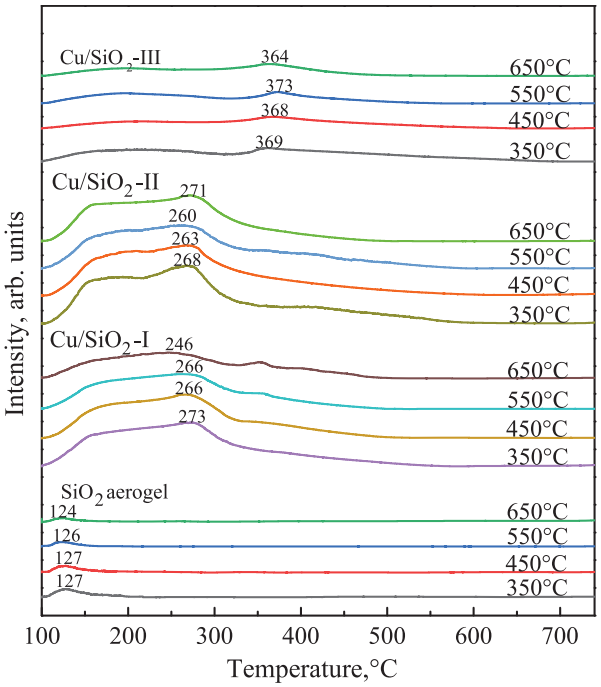

Fig. 5. NH_3-TPD profiles of the reduced Cu/SiO_2 catalysts and SiO_2 aerogel.

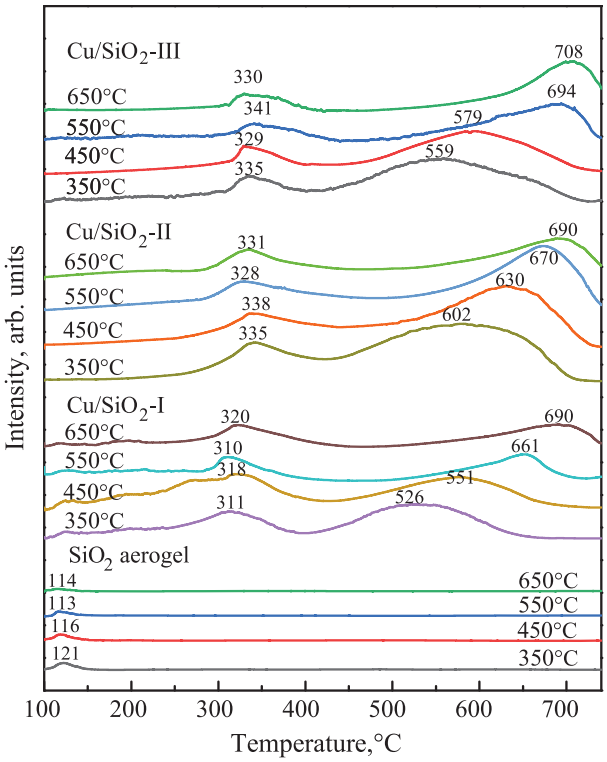

Fig. 6. CO_2-TPD profiles of the reduced Cu/SiO_2 catalysts and SiO_2 aerogel.

symmetrical peaks using a XPSPEAK41 software. By deconvolution of the XAES peaks, the area ratios of the surface Cu^+ to Cu^0 of the Cu/SiO_2-III-350°C and Cu/SiO_2-III-650°C catalysts were 1 : 0.23 and 1 : 0.07, respectively. The results indicated that the surface oxidation state of the copper species in the reduced Cu/SiO_2 catalysts was influenced by the calcination temperatures of their CuO/SiO_2 precursors.

Specific Surface Area and Pore Size of Reduced Cu/SiO$_2$ Catalyst

The specific surface areas and average pore diameters of the reduced Cu/SiO_2 catalysts were around 155 $m^2\ g^{-1}$ and 15 nm, respectively (Table 1). The SiO_2 aerogel endowed the catalysts with a large surface area and pore diameter. The calcination temperature ranging from 350 to 650°C had no obvious effect on surface area and pore size.

Acidity and Basicity of Reduced Cu/SiO$_2$ Catalyst

The NH_3-TPD profiles of the calcined SiO_2 aerogel and reduced Cu/SiO_2 catalysts are shown in Fig. 5. For the calcined SiO_2 aerogel, a very weak NH_3 desorption peak appeared at 126°C, indicating that the SiO_2 aerogel had weak acid acidity and weak-strength acid sites. The acidity of the SiO_2 aerogel decreased with the increase of the calcination temperatures (Table 1).

The NH_3 desorption peaks of the reduced Cu/SiO_2-I and Cu/SiO_2-II catalysts appeared in a wide temperature range of 110–350°C, indicating that the reduced Cu/SiO_2-I and Cu/SiO_2-II catalysts had weak- and medium-strength acid sites. For the reduced Cu/SiO_2-III catalysts, their NH_3 desorption peaks were weak and appeared at the temperature of around 370°C. The Cu/SiO_2-III catalysts had a lower acidity and medium-strength acid sites.

The total acidities of the reduced Cu/SiO_2 catalysts were in an order of Cu/SiO_2-II > Cu/SiO_2-I > Cu/SiO_2-III >> SiO_2 (Table 1). The precipitation procedures obviously affected the total acidity of the reduced Cu/SiO_2 catalyst. In addition, when the catalyst precursor, CuO/SiO_2 was calcined at a higher temperature, the reduced Cu/SiO_2 catalyst had a lower total acidity.

The CO_2-TPD profiles of the reduced Cu/SiO_2 catalysts and SiO_2 aerogel are shown in Fig. 6. Their

total basicities are listed in Table 1. For the SiO_2 aerogel calcined at different temperatures, a very weak CO_2 desorption peak appeared at 116°C, indicating that the calcined SiO_2 samples had a lower basicity and weak-strength basic sites. For all the reduced Cu/SiO_2-I, Cu/SiO_2-II, and Cu/SiO_2-III catalysts, two CO_2 desorption peaks appeared at 310–341 and 526–708°C, respectively. The reduced Cu/SiO_2 catalysts had both medium- and strong-strength basic sites. The CO_2 desorption peaks of the strong-strength basic sites shifted to high temperatures upon increasing the calcination temperatures, indicating that the high calcination temperature endowed the Cu/SiO_2 catalyst with stronger basic strength.

The total basicities of the reduced Cu/SiO_2 catalysts were in an order of Cu/SiO_2-II > Cu/SiO_2-III > Cu/SiO_2-I >> aerogel SiO_2 (Table 1). The direct precipitation method favored the formation of Cu/SiO_2 catalysts with a lower total basicity. Although the high calcination temperature endowed the catalysts with stronger basic strength, the total basicity decreased upon increasing the calcination temperature.

According to the NH_3- and CO_2-TPD analyses, it could be reasonable to conclude that the acidity and basicity of the reduced Cu/SiO_2 catalysts were ascribed to the interaction between metallic copper species and SiO_2 support rather than the sole aerogel SiO_2 support. Unavoidably, the precipitation procedures and calcination temperature affected the interaction between copper species and SiO_2 support, which subsequently influenced the acidity and basicity of the reduced Cu/SiO_2 catalyst.

Catalytic Performance of Cu/SiO_2 Catalyst

The catalytic performance of the reduced Cu/SiO_2 catalysts for the dehydrogenation of methanol to methyl formate at the reaction temperatures ranging from 200 to 280°C was investigated. The main products were methyl formate, CO, and H_2. The conversion of methanol, selectivity of methyl formate, and selectivity of CO over the Cu/SiO_2 catalysts are shown in Figs. 7 and 8, respectively.

When the reduced Cu/SiO_2-I catalysts prepared through the calcination at different temperatures of 350–650°C were used for the methanol dehydrogenation reaction at the reaction temperature of 200°C, the methanol conversions increased from 19.8% to 23.8% upon increasing the calcination temperatures. At the reaction temperature of 280°C, the methanol conversions increased from 52.0 to 59.2%.

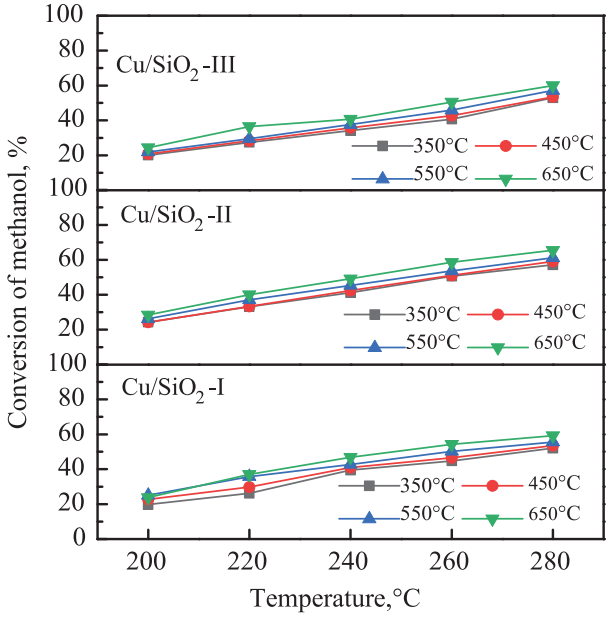

Fig. 7. Methanol conversion in the methanol dehydrogenation reaction catalyzed by the reduced Cu/SiO_2 catalysts

When the reduced Cu/SiO_2-II catalysts prepared through the calcination at the temperatures of 350–650°C were used for the methanol dehydrogenation reaction at the reaction temperature of 200°C, the methanol conversions increased from 24.3 to 28.4% upon increasing the calcination temperatures. At the reaction temperature of 280°C, the methanol conversions increased from 57.1 to 65.5%.

Over the Cu/SiO_2-III catalysts, at the reaction temperature of 200°C, the methanol conversions increased from 20.1 to 24.5% when increasing the calcination temperatures of their catalyst precursors from 350 to 650°C. When the reaction temperature was raised to 280°C, the methanol conversions increased from 52.9 to 60.0%.

The catalytic activity for the methanol conversion was in an order of Cu/SiO_2-II > Cu/SiO_2-III > Cu/SiO_2-I. The reduced Cu/SiO_2 catalysts with the small-sized copper crystallites exhibited higher catalytic activity for methanol conversion. High calcination temperature for the catalyst precursor or high reaction temperature was beneficial to the methanol dehydrogenation reaction.

The selectivity of methyl formate decreased whereas the selectivity of CO increased in the methanol dehydrogenation reaction catalyzed by the reduced Cu/SiO_2 catalysts with the increase in the reaction temperature (Fig. 8).

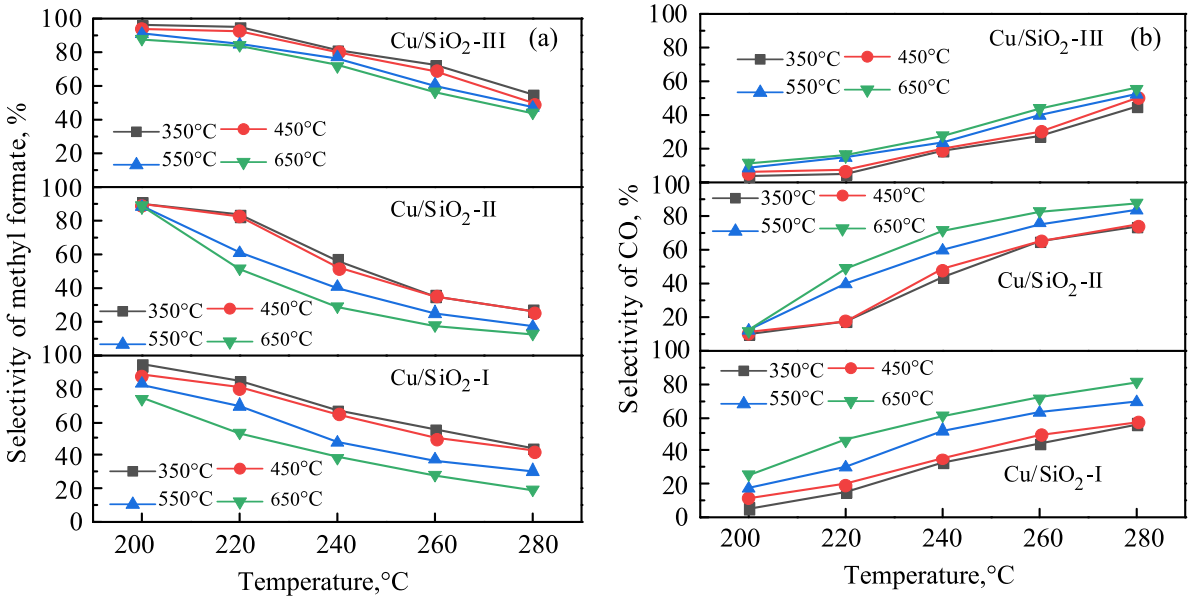

Fig. 8. Selectivities of (a) methyl formate and (b) CO in the methanol dehydrogenation reaction catalyzed by Cu/SiO_2 catalysts.

When the reduced Cu/SiO_2-I catalysts catalyzed the methanol dehydrogenation reaction, at the reaction temperature of 200°C, the selectivities of methyl formate decreased from 93.9% to 74.0% with the increase in the calcination temperatures of the catalyst precursors from 350 to 650°C. Only CO and H_2 as the byproducts were detected under our present experimental conditions and the selectivities of CO increased from 6.1 to 26.0% with the increase in the calcination temperatures. At the reaction temperature of 280°C, the selectivities of methyl formate decreased from 44.0 to 19.3% whereas the selectivities of CO increased from 56.0% to 80.7% with the increase in the calcination temperatures.

For the reduced Cu/SiO_2-II catalysts, at the reaction temperature of 200°C, the selectivities of methyl formate decreased from 90.3 to 88.4% and the selectivites of CO increased from 9.7 to 11.6% with increasing the calcination temperatures. At the reaction temperature of 280°C, the selectivities of methyl formate decreased from 26.3 to 12.4% while the selectivities of CO increased from 73.7 to 87.6% with increasing the calcination temperatures.

Over the reduced Cu/SiO_2-III catalysts at the reaction temperature of 200°C, the selectivities of methyl formate decreased from 96.3 to 88.2% with increasing the calcination temperatures. The selectivities of CO ranged from 3.7 to 11.8%. At the reaction temperature of 280°C, the selectivities of methyl formate decreased from 55.2 to 44.3% and the selectivities of CO increased from 44.8 to 55.7% with increasing the calcination temperatures.

The selectivity of methyl formate was in an order of Cu/SiO_2-III > Cu/SiO_2-I > Cu/SiO_2-II. It could be explained as that the reduced Cu/SiO_2-III catalyst had a relative lower acidity and basicity, inhibiting the decomposition of resultant methyl formate to CO and H_2 [17]. Otherwise, the reduced Cu/SiO_2-II catalyst with a higher acidity and basicity could enhance the decomposition of resultant methyl formate to CO and H_2, giving a lower selectivity of methyl formate.

When the CuO/SiO_2 precursors were prepared at a higher calcination temperature, the reduced Cu/SiO_2 catalysts gave a higher methanol conversion but a lower methyl formate selectivity. Combining the surface Cu^+/Cu^0 ratios of copper species in the reduced Cu/SiO_2 catalysts, it was reasonable to suggest that the surface metallic Cu^0 and Cu^+ cations at the catalyst surface probably catalyzed the dehydrogenation of methanol, meanwhile the Cu^+ cations enhanced the decomposition of the resultant formate. The similar phenomenon was also observed by the other researchers using *in situ* DRIFT technique [7].

CONCLUSIONS

When the Cu/SiO_2 catalysts were prepared by the reverse and co-current flow precipitation procedures, the small-sized copper nanocrystallites were formed

after reduction with gaseous hydrogen, giving a higher methanol conversion. The direct precipitation caused the formation of large-sized copper nanocrystallites, giving a lower methanol conversion.

The reverse precipitation method endowed the reduced Cu/SiO_2 catalysts with a lower acidity and basicity, favoring the methanol dehydrogenation to methyl formate.

High calcination temperature resulted in a strong interaction between copper species and SiO_2 aerogel, improving the methanol conversion as well as the decomposition of resultant methyl formate to CO and H_2.

ACKNOWLEDGMENTS

This work was financially supported by the Jiangsu Science and Technology Department, China (FZ20180919).

CONFLICT OF INTEREST

The authors state that they have no conflict of interest to be disclosed in the present communication.

REFERENCES

1. Huang, C., Wen, J., Sun, Y., Zhang, M., Bao, Y., Zhang, Y., Liang, L., Fu, M., Wu, J., Ye, D., and Chen, L., *Chem. Eng. J.*, 2019, vol. 374, pp. 221–230. https://doi.org/10.1016/j.cej.2019.05.123
2. Du, H., Ma, X., Yan, P., Jiang, M., Zhao, Z., and Zhang, Z.C., *Fuel Process. Technol.*, 2019, vol. 193, pp. 221–231. https://doi.org/10.1016/j.fuproc.2019.05.003
3. Zhang, D., Yin, H., Ge, C., Xue, J., Jiang, T., Yu, L., and Shen, Y., *J. Ind. Eng. Chem.*, 2009, vol. 15, pp. 537–543. https://doi.org/10.1016/j.jiec.2009.01.010
4. Zhang, D., Yin, H., Xue, J., Ge, C., Jiang, T., Yu, L., and Shen, Y., *Ind. Eng. Chem. Res.*, 2009, vol. 48, pp. 11220–11224. https://doi.org/10.1021/ie9013875
5. Ferrah, D., Haines, A.R., Galhenage, R.P., Bruce, J.P., Babore, A.D., Hunt, A., Waluyo, I., and Hemminger, J.C., *ACS Catal.*, 2019, vol. 9, pp. 6783−6802. https://doi.org/10.1021/acscatal.9b01419
6. Lu, Z., Yin, H., Wang, A., Hu, J., Xue, W., Yin, H., and Liu, S., *J. Ind. Eng. Chem.*, 2016, vol. 37, pp. 208–215. https://doi.org/10.1016/j.jiec.2016.03.028
7. Yang, H., Chen, Y., Cui, X., Wang, G., Cen, Y., Deng, T., Yan, W., Gao, J., Zhu, S., Olsbye, U., Wang, J., and Fan, W., *Angew. Chem.*, 2018, vol. 130, pp. 1854–1858. https://doi.org/10.1002/anie.201710605
8. Salaeva, A.A., Salaev, M.A., Vodyankina, O.V., and Mamontov, G.V., *Appl. Catal. A.*, 2019, vol. 581, pp. 82–90. https://doi.org/10.1016/j.apcata.2019.05.018
9. Yin, H., Yin, H., Wang, A., Shen, L., Liu, Y., and Zheng, Y., *J. Nanosci. Nanotechnol.*, 2017, vol. 17, pp. 1255–1266. https://doi.org/10.1166/jnn.2017.12573
10. Park, J., Cho, J., Lee, Y., Park, M.J., and Lee, W.B., *Ind. Eng. Chem. Res.*, 2019, vol. 58, pp. 8663–8673. https://doi.org/10.1021/acs.iecr.9b01254
11. Sitthisa, S., Sooknoi, T., Ma, Y., Balbuena, P.B., and Resasco, D.E., *J. Catal.*, 2011, vol. 277, pp. 1–13. https://doi.org/10.1016/j.jcat.2010.10.005
12. Indu, B., Ernst, W.R., and Gelbaum, L.T., *Ind. Eng. Chem. Res.*, 1993, vol. 32, pp. 981–985. https://doi.org/10.1021/ie00017a031
13. He, L., Liu, H., Xiao, C., and Kou, Y., *Green Chem.*, 2008, vol. 10, pp. 619–622. https://doi.org/10.1039/B804459G
14. Ai, M., *J. Catal.*, 1982, vol. 77, pp. 279–288. https://doi.org/10.1016/0021-9517(82)90168-3
15. Shelepova, E.V., Ilina, L.Y., and Vedyagin, A.A., *Catal. Today*, 2019, vol. 331, pp. 35–42. https://doi.org/10.1016/j.cattod.2017.11.023
16. Matsuda, T., Yogo, K., Pantawong, C., and Kikuchi, E., *Appl. Catal. A.*, 1995, vol. 126, pp. 177–186. https://doi.org/10.1016/0926-860X(95)00041-0
17. Lu, Z., Gao, D., Yin, H., Wang, A., and Liu, S., *J. Ind. Eng. Chem.*, 2015, vol. 31, pp. 301–308. https://doi.org/10.1016/j.jiec.2015.07.002
18. Shelepova, E.V., Vedyagin, A.A., Ilina, L.Y., Nizovskii, A.I., and Tsyrulnikov, P.G., *Appl. Surf. Sci.*, 2017, vol. 409, pp. 291–295. https://doi.org/10.1016/j.apsusc.2017.02.220
19. Zhang, R., Sun, Y., and Peng, S., *Fuel*, 2002, vol. 81, pp. 1619–1624. https://doi.org/10.1016/S0016-2361(02)00085-6
20. Minyukova, T.P., Simentsova, I.I., Khasin, A.V., Shtertser, N.V., Baronskaya, N.A., Khassin, A.A., and Yurieva, T.M., *Appl. Catal. A.*, 2002, vol. 237, pp. 171–180. https://doi.org/10.1016/S0926-860X(02)00328-9
21. Guerreiro, E.D., Gorriz, O.F., Larsen, G., and Arrúa, L.A., *Appl. Catal. A.*, 2000, vol. 204, pp. 33–48. https://doi.org/10.1016/S0926-860X(00)00507-X
22. Guo, Y., Lu, G., Mo, X., and Wang, Y., *Catal. Lett.*, 2005, vol. 99, pp. 105–108. https://doi.org/10.1007/s10562-004-0783-3

23. Kipnis, M.A., Volnina, E.A., Belostotskii, I.A., and Levin, I.S., *Kinet. Catal.*, 2020, vol. 61, pp. 145–154. https://doi.org/10.1134/S0023158420010024

24. Zhong, J., Yang, X., Wu, Z., Liang, B., Huang, Y., and Zhang, T., *Chem. Soc. Rev.*, 2020, vol. 49, pp. 1385–1413. https://doi.org/10.1039/C9CS00614A

25. Minyukova, T.P., Khasin, A.V., Khassin, A.A., Shtertser, N.V., Simentsova, I.I., and Yurieva, T.M., *Catal. Ind.*, 2016, vol. 8, pp. 293–299. https://doi.org/10.1134/S2070050416040073

26. Xue, W., Yin, H., Lu, Z., Wang, A., Liu, S., and Shen, L., *J. Nanosci. Nanotechnol.*, 2018, vol. 18, pp. 3362–3372. https://doi.org/10.1166/jnn.2018.14706

27. Yin, H., Zhang, C., Yin, H., Gao, D., Shen, L., and Wang, A., *Chem. Eng. J.*, 2016, vol. 288, pp. 332–343. https://doi.org/10.1016/j.cej.2015.12.010

28. Wang, A., Zhang, M., Yin, H., Liu, S., Liu, M., and Hu, T., *RSC Adv.*, 2018, vol. 8, pp. 19317–19325. https://doi.org/10.1039/C8RA03125H

29. Dai, W.L., Sun, Q., Deng, J.F., Wu, D., and Sun, Y.H., *Appl. Surf. Sci.*, 2001, vol. 177, pp. 172–179. https://doi.org/10.1016/S0169-4332(01)00229-X

30. Aravinda, C.L., Bera, P., Jayaram, V., Sharma, A.K., and Mayanna, S.M., *Mater. Res. Bull.*, 2002, vol. 37, pp. 397–405. https://doi.org/10.1016/S0025-5408(01)00821-2

31. Deutsch, K.L., and Shanks, B.H., *Appl. Catal. A.*, 2012, vol. 447–448, pp. 144–150. https://doi.org/10.1016/j.apcata.2012.09.047

32. Sun, K., Lu, W., Qiu, F., Liu, S., and Xu, X., *Appl. Catal. A.*, 2003, vol. 252, pp. 243–249. https://doi.org/10.1016/S0926-860X(03)00466-6*A*